Multi-scale fibre-based optical frequency combs: science, technology and applications (MEFISTA)

Deliverables D4.2

Equations with reduced complexity for theoretical characterisation of the polarisation dynamics of EOFC, numerical codes, results of numerical modelling and simplified analytical approaches to the polarisation dynamics of the mode-locked lasers.

Project details

Project Number	861152	Project Acronym	MEFISTA
Project Title	Multi-scale fibre-based optical frequency combs: science, technology and applications		
Project website	https://mefista.astonphotonics.uk/		
Starting date	01/02/2020		
Project duration	48		
Call (part) identifier	H2020-MSCA-ITN-2019		
Topic	MSCA-ITN-2019 Innovative Training Network		

Document details

Title	Equations with reduced complexity for theoretical characterisation of the polarisation dynamics of EOFC, numerical codes, results of numerical modelling and simplified analytical approaches to the polarisation dynamics of the mode-locked lasers.		
Deliverable number		Deliverable Rel. number	D4.2
Work Package	WP4		
Deliverable type	Report		
Description	Equations with reduced complexity for theoretical characterisation of the polarisation dynamics of EOFC, numerical codes, results of numerical modelling and simplified analytical approaches to the polarisation dynamics of the mode-locked lasers.		
Deliverable due date	31st January 2021		
Actual date of submission	13 October 2022		
Lead beneficiary	Aston		
Version number	V2.0		
Status	Completed		

Dissemination level

Public (PU)	X
Confidential, only for members of the consortium (including Commission Services)	

Contents

List of Figures

EXECUTIVE SUMMARY

- Due to covid travel restriction and delayed recruitment of ESR4 and ESR5, the D4.2 was partially completed to the deadline of 31st January 2022.
- New model of Er-doped fibre laser accounting for electrostriction effect leading to excitation of the torsional acoustic modes in the transverse section of the laser has been developed to explain experimental data on harmonic mode-locking. These results have been published in the Photonics Research journal.
- ESR 4 contributed to development of new theoretical model of complex polarisation dynamics in Er-doped fibre laser mode-locked based on nonlinear polarisation rotation (NPR). Results of the theoretical modelling are in use to explain experimentally observed polarisation dynamics.
- In the next 3-4 months, the model will be updated by ESR4 and ESR5 to characterise the polarization dynamics of dual-comb mode-locked fibre laser towards tunability of the polarisation attractors, repetition rate and difference in repetition rates.

CONTENT

In this report, for Er-doped fibre lasers, we summarise development and tests of theoretical models for explanation of the experimental results on vector harmonic mode locking, tunability of the polarisation attractors in the lasers mode-locked by nonlinear polarisation rotation.

Vector harmonic mode-locking (HML) by acoustic resonance [1]

To understand the mechanism of vector mode-locking caused by stable self-mode locking and tunability of harmonic mode-locking and linewidth narrowing, we developed a new vector model of EDFLs as described in the ref. [1]. The model accounts for the linear and circular birefringence and fast- and slow axis modulation caused by torsional-radial (TR_{2m}) acoustic modes. Without accounting for the gain dynamics, the SOP evolution in terms of the Stokes vector *S* and number of roundtrips caused by the interplay of the factors mentioned above can be described as follows:

$$\boldsymbol{dS/dt = R \cdot W \times S}, \tag{1}$$

Here time is normalized to the roundtrip time, $W = (\beta_L, 0, \beta_c)^T$ is the birefringence vector, $\beta_{L\,(C)} = 2\pi/L_{bL(bC)}$ is the linear (circular) birefringence strength, $L_{bL(bC)}$ is the beat length for linear (circular) birefringence. The matrix R is the 3x3 matrix that defines the rotation of the birefringence vector around axis OS_3 caused by TR_{2m} excitation [1]:

$$\boldsymbol{R} = \begin{bmatrix} \boldsymbol{\cos\left(\zeta(t)\right)} & \boldsymbol{-\sin\left(\zeta(t)\right)} & \boldsymbol{0} \\ \boldsymbol{\sin\left(\zeta(t)\right)} & \boldsymbol{\cos\left(\zeta(t)\right)} & \boldsymbol{0} \\ \boldsymbol{0} & \boldsymbol{0} & \boldsymbol{1} \end{bmatrix}, \tag{2}$$

where $\zeta(t) = A_0 \cos(2\pi\Omega t)$. Here $\zeta(t)$ is the angle of the birefringence vector rotation, A_0 is the amplitude of rotation, and Ω is the frequency of oscillations at the TR_{2m} acoustic mode. In Eqs. 1 and 2, the contribution of TR_{2m} was accounting for only in the birefringence modulation context. The modulation of the refractive index was neglected. Given the complexity of the problem, we introduced a few approximations to reveal the effect of the TR_{2m} on the modulation of the output power at frequency Ω, resulting in HML if the frequency Ω coincides with the frequency of the harmonic q. First, though the TR_{2m} modulates all modes that result in HML stabilization shown in [1], in the theoretical analysis, we accounted for the only interplay of the linear and circular birefringence with the TR_{2m} acoustic mode-based modulation for harmonic $q = 0$ in terms of the ability of excitation of the output power oscillations at a frequency of TR_{2m} mode [1].

The results of the theoretical analysis are shown in Fig. 1 (a-i). As follows from Figs. 1 (a), (b); (d), (e), the output power I and I_x, I_y are oscillating at frequency $\omega = \sqrt{\beta_L^2 + \beta_c^2}$ [1], whereas oscillations at the frequency Ω have almost been suppressed. Only for the case when the frequency $\Omega = 14\pi$ is a multiple of frequency $\omega = 2\pi$, the oscillations at the frequency ω disappear, and the output power is modulated at frequency Ω. This is like the experimental data shown in Fig. 1, where HML is stabilized only when $\omega = 2\pi$, i.e. when the satellites' frequencies are matching the frequency spacing between harmonics. The HML mechanism looks like the vector mode-locking at the fundamental frequency [1]. By adjusting the in-cavity polarization controller, we were able to increase the circular birefringence strength that leads to the generation of two satellite lines around the q=0 harmonic frequency. When the birefringence-based modulation frequency ω approaches the fundamental frequency, the modulation of the harmonic at the frequency ω disappears, and TR_{2m} is activation results in modulation of q=0 cavity mode with the frequency of TR_{2m}. The amplitude of the output power (Fig. 1 g) along with the Stokes parameters shown was small, and so SOP was locked (Fig. 4 (i)).

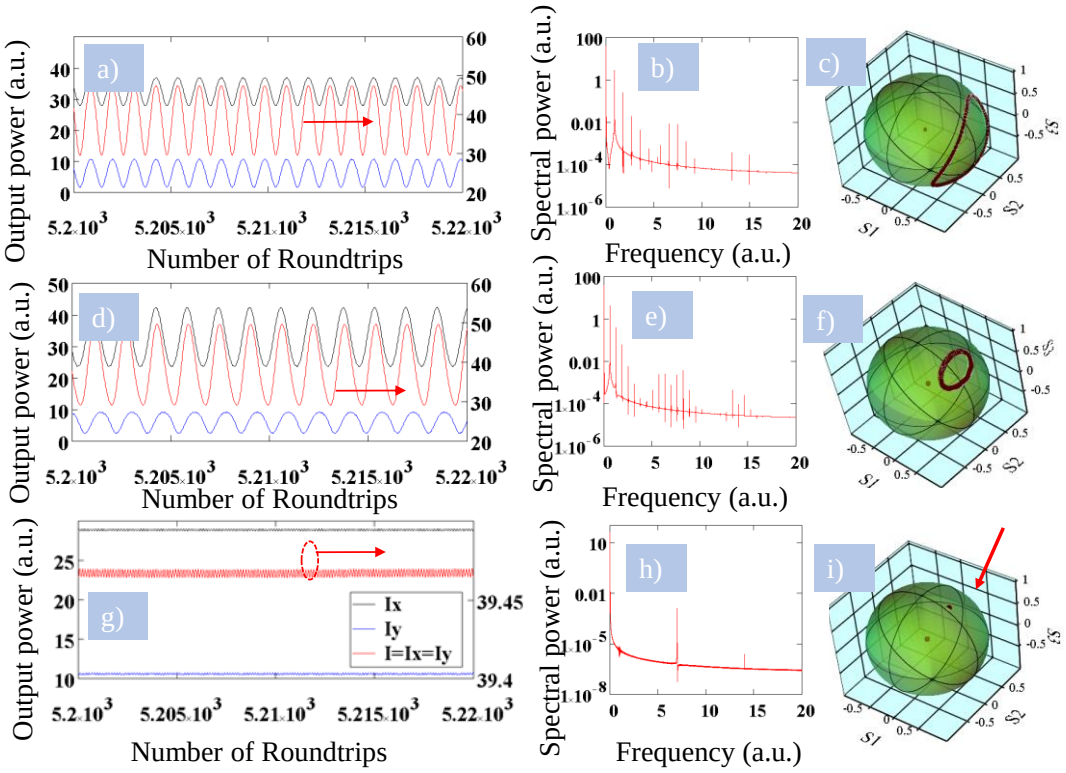

Fig. 1. Results of the numerical modeling. a), d), g) The output power vs time for two linearly cross-polarized SOPs I_x (blue line) and I_y (black) and total power $I=I_x+I_y$(red); b), e), h) Spectrum of the oscillations; c), f), i) trajectories on the Poincare sphere. Parameters: time is normalized to the roundtrip time, frequency Ω – to the fundamental frequency; birefringence strengths β_L, β_C - to the fiber length.

Vector model of a fibre laser mode-locked based on Nonlinear Polarisation Rotation (NPR)

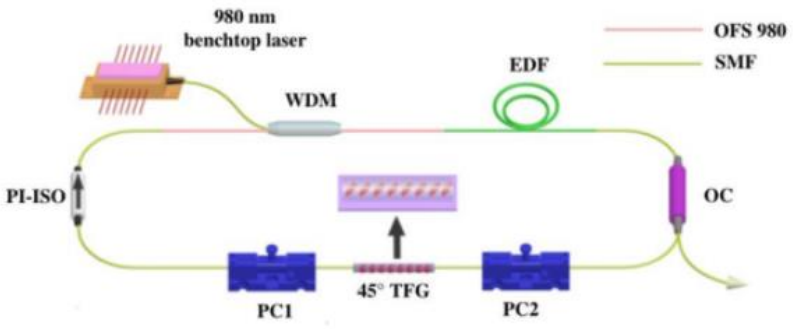

Fig. 2. Schematic setup of the NPR mode-locked fibre laser.

To characterize the polarization dynamics of the system shown in Fig.2, we use the vector model of Erbium-doped fiber laser for the cross-polarized (x and y) components of the lasing field u and v, averaged over the pulse width and combined with the model of NPR mode-locking [1]:

$$\frac{du}{dt} = i\beta u + i\frac{\gamma}{2}\left(|u|^2u + \frac{2}{3}|v|^2u + \frac{1}{3}v^2u^*\right) + (D_{xx} + a_{11})u + (D_{xy} + a_{12})v,$$

$$\frac{dv}{dt} = -i\beta v + i\frac{\gamma}{2}\left(|v|^2v + \frac{2}{3}|u|^2v + \frac{1}{3}u^2v^*\right) + (D_{xy} + a_{21})u + (D_{yy} + a_{22})v,$$

$$\frac{dn_0}{dt} = \varepsilon\left[I_p + 2R_{10} - \left(1 + \frac{I_p}{2} + \chi R_{10}\right)n_0 - \chi R_{11}n_{12} - \chi n_{22}R_{12}\right],$$

$$\frac{dn_{12}}{dt} = \varepsilon\left[\frac{(1-\delta^2)}{(1+\delta^2)}\frac{I_p}{2} + R_{11} - \left(1 + \frac{I_p}{2} + \chi R_{10}\right)n_{12} - \left(\frac{(1-\delta^2)}{(1+\delta^2)}\frac{I_p}{2} + \chi R_{11}\right)\frac{n_0}{2}\right],$$

$$\frac{dn_{22}}{dt_s} = \varepsilon\left[R_{12} - \left(1 + \frac{I_p}{2} + \chi R_{10}\right)n_{22} - \chi R_{12}\frac{n_0}{2}\right],$$

$$R_{10} = \frac{1}{(1+\Delta^2)}(|u|^2 + |v|^2), \quad R_{11} = \frac{1}{(1+\Delta^2)}(|u|^2 - |v|^2), R_{12} = \frac{1}{(1+\Delta^2)}(uv^* + vu^*), \tag{1}$$

Coefficients D_{ij} can be found as follows:

$$D_{xx} = \frac{\alpha_1(1-i\Delta)}{1+\Delta^2}(f_1 + f_2) - \alpha_2,\ D_{yy} = \frac{\alpha_1(1-i\Delta)}{1+\Delta^2}(f_1 - f_2) - \alpha_2, \tag{2}$$

$$D_{xy} = D_{yx} = \frac{\alpha_1(1-i\Delta)}{1+\Delta^2}f_3,$$

where:

$$f_1 = \left(\chi\frac{n_0}{2} - 1\right),\ f_2 = \chi\frac{n_{12}}{2},\ f_3 = \chi\frac{n_{22}}{2}. \tag{3}$$

$$a_{ij} = ln(T)_{ij}, T = T_{POC1}\cdot T_{TFG}\cdot T_{POC2}\quad i,,j = 1,2,$$

$$T_{POC1(2)} = \begin{bmatrix} exp\left(\frac{i\varphi_{1(2)}}{2}\right)cos\left(\xi_{1(2)}\right) & exp\left(\frac{i\varphi_{1(2)}}{2}\right)sin\left(\xi_{1(2)}\right) \\ exp\left(-\frac{i\varphi_{1(2)}}{2}\right)sin\left(\xi_{1(2)}\right) & exp\left(-\frac{i\varphi_{1(2)}}{2}\right)cos\left(\xi_{1(2)}\right) \end{bmatrix}, T_{TFG} = \begin{bmatrix} cos(\theta) & 0 \\ 0 & sin(\theta) \end{bmatrix}. \tag{4}$$

Here time t is normalized to the round-trip time τ_r; $|u|^2$, $|v|^2$ are normalized to the saturation power I_{ss} and I_p is normalized to the saturation power I_{ps}, α_1 is the total absorption of erbium ions at the lasing wavelength; α_2 represents the normalized losses; δ is the ellipticity of the pump wave, $\varepsilon=\tau_r/\tau_{Er}$ is the ratio of the round-trip time τ_r to the lifetime of erbium ions at the first excited level τ_{Er}; $\chi_{p,s}=(\sigma_a^{(s,p)}+\sigma_e^{(s,p)})/\sigma_a^{(s,p)}$,($\sigma_a^{(s,p)}$ and $\sigma_e^{(s,p)}$are absorption and emission cross-sections at the lasing (s) and pump (p) wavelengths); Δ is the detuning of the lasing wavelength with respect to the maximum of the gain spectrum (normalized to the gain spectral width), β is the birefringence strength ($2\beta=2\pi L_c/L_b$, L_b is the beat length and L_c is the cavity length), $T_{POC1(2)}$ and T_{TFG} are Jones matrices describing SOP transformation by POC1, POC2 and 45^0 TFG, where $\xi_{1(2)}$is the angle of rotation of the vertical birefringent axis and

$\varphi_{1(2)}$ is the phase shift between the wave components in the two orthogonal birefringent axes, the angle between the axis of the polarizer (45°-TFG) and the y axis is θ.

The following preliminary tests have been completed to find solutions close to the experimental results [2].

Test 1

Parameters: $a_{11}=\ln(0.924)$, $a_{12}=a_{21}=0$, $a_{22}=\ln(0.393)$, Pump power: $I_p=80$, $a_1=11.052$; $\varepsilon=10^{-4}$; $\beta=0$; $\alpha_2=2.553$; $\Delta=0.15$; $\chi=2.3$; $\gamma=2\cdot10^{-6}$; $\delta=0.99$.

Test 2

Parameters: $a_{11}=\ln(0.951)$, $a_{12}=a_{21}=0$, $a_{22}=\ln(0.309)$, Pump power: $I_p=80$, $a_1=11.052$; $\varepsilon=10^{-4}$; $\beta=0$; $\alpha_2=2.553$; $\Delta=0.15$; $\chi=2.3$; $\gamma=2\cdot10^{-6}$; $\delta=0.8$.

Test 3

Parameters: $a_{11}=\ln(0.988)$, $a_{12}=a_{21}=0$, $a_{22}=\ln(0.156)$, Pump power: $I_p=80$, $a_1=11.052$; $\varepsilon=10^{-4}$; $\beta=0$; $\alpha_2=2.553$; $\Delta=0.15$; $\chi=2.3$; $\gamma=2\cdot10^{-6}$; $\delta=0.97$.

Results

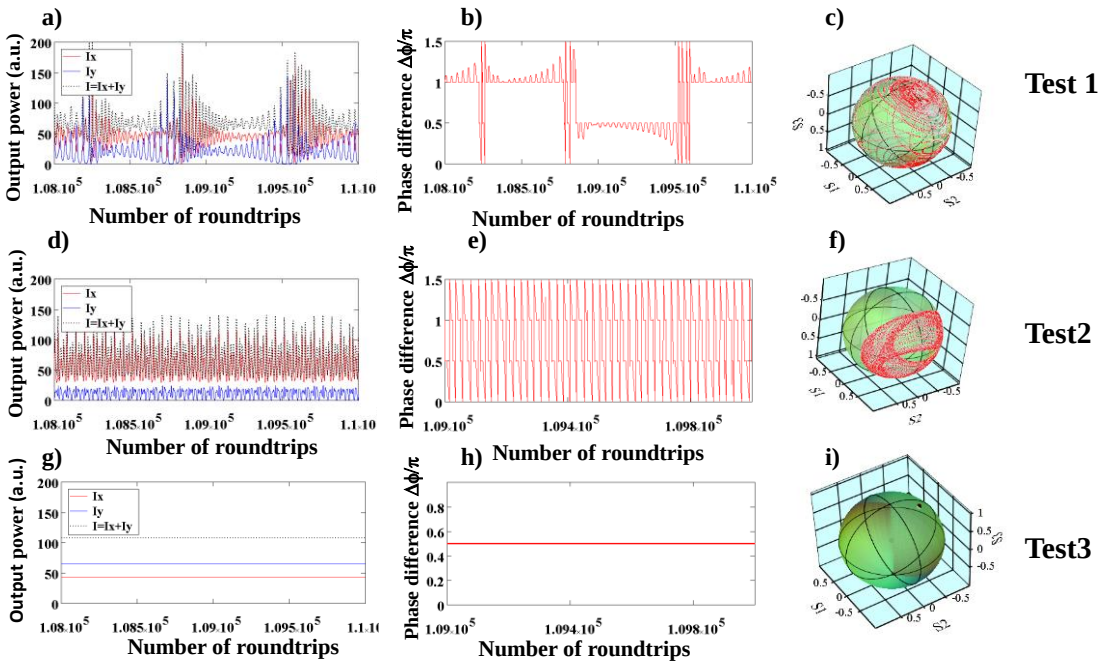

Figure 3. Evolution of the pulse energy and the state of polarization for nonlinear polarization rotation-based mode-locked laser. $I_x = |u|^2$, $I_y = |v|^2$ as a function of time (Number of roundtrips).

$S_0 = |u|^2 + |v|^2, S_1 = |u|^2 - |v|^2, S_2 = (uv^* + vu^*), S_3 = -i(uv^* + vu^*), \quad s_i = \frac{S_i}{\sqrt{S_1^2+S_2^2+S_3^2}}, (i = 1, 2, 3).$

$\Delta\phi = \operatorname{atan}(S_3/S_2)$.

Vector model of mode-locked fibre laser with injected signal

To understand the mechanism of polarization attractor evolution caused by drifting soliton rain, we developed a new vector model of EDFLs from the vector theory developed by Sergeyev and co-workers [3]. The model accounts for the linear and circular birefringence and evolution of the laser SOPs and the first excited level population in Er^{3+} doped active medium. The previous model was complemented by the model of the vector soliton rain in the form of an injected signal with periodically evolving orthogonal states of polarization:

$$\boldsymbol{E_x = a \cdot \cos(\Omega t + \phi_0)}, \boldsymbol{E_y = a \cdot \sin(\Omega t + \phi_0) \cdot exp(\Delta\varphi)}. \quad (5)$$

Here a is the amplitude of the soliton rain, W is the frequency of oscillations, and f_0 is the initial phase, $\Delta\varphi$ is the phase difference between the orthogonal SOPs. The model is inspired by the idea that the main pulse produces the polarization hole burning in the orientation distribution of inversion and so SR pulses have SOPs different from the main pulse's SOP [3]. Periodically evolving SOP of the main pulse leads to the oscillation of the SR SOP as shown in Eq. 5. With taking into account Eq. (5), the model can be presented as follows [3]:

$$\begin{gathered}
\frac{du}{dt} = i\beta u + i\frac{\gamma}{2}\left(|u|^2u + \frac{2}{3}|v|^2u + \frac{1}{3}v^2u^*\right) + D_{xx}u + D_{xy}v + E_x, \\
\frac{dv}{dt} = -i\beta v + i\frac{\gamma}{2}\left(|v|^2v + \frac{2}{3}|u|^2v + \frac{1}{3}u^2v^*\right) + D_{xy}u + D_{yy}v + E_y, \\
\frac{dn_0}{dt} = \varepsilon\left[I_p + 2R_{10} - \left(1 + \frac{I_p}{2} + \chi R_{10}\right)n_0 - \chi R_{11}n_{12} - \chi n_{22}R_{12}\right], \\
\frac{dn_{12}}{dt} = \varepsilon\left[\frac{(1-\delta^2)}{(1+\delta^2)}\frac{I_p}{2} + R_{11} - \left(1 + \frac{I_p}{2} + \chi R_{10}\right)n_{12} - \left(\frac{(1-\delta^2)}{(1+\delta^2)}\frac{I_p}{2} + \chi R_{11}\right)\frac{n_0}{2}\right], \\
\frac{dn_{22}}{dt_s} = \varepsilon\left[R_{12} - \left(1 + \frac{I_p}{2} + \chi R_{10}\right)n_{22} - \chi R_{12}\frac{n_0}{2}\right], \\
R_{10} = \frac{1}{(1+\Delta^2)}(|u|^2 + |v|^2), \quad R_{11} = \frac{1}{(1+\Delta^2)}(|u|^2 - |v|^2), R_{12} = \frac{1}{(1+\Delta^2)}(uv^* + vu^*),
\end{gathered} \quad (6)$$

Coefficients D_{ij} can be found as follows:

$$\begin{gathered}
D_{xx} = \frac{\alpha_1(1-i\Delta)}{1+\Delta^2}(f_1 + f_2) - \alpha_2 + ln\left(1 - \frac{\alpha_0}{1+\alpha_s(|u|^2+v^2)}\right), \; D_{yy} = \frac{\alpha_1(1-i\Delta)}{1+\Delta^2}(f_1 - f_2) - \alpha_2 + \\
ln\left(1 - \frac{\alpha_0}{1+\alpha_s(|u|^2+v^2)}\right), D_{xy} = D_{yx} = \frac{\alpha_1(1-i\Delta)}{1+\Delta^2}f_3.
\end{gathered} \quad (7)$$

where:

$$f_1 = \left(\chi\frac{n_0}{2} - 1\right), \; f_2 = \chi\frac{n_{12}}{2}, \; f_3 = \chi\frac{n_{22}}{2}. \quad (8).$$

Here time t is normalized to the photon lifetime in the cavity τ_p, $I_x=/u/^2$, $I_y=/v/^2$ are normalized to the saturation power I_{ss} and I_p is normalized to the saturation power I_{ps}, α_1 is the total absorption of erbium ions at the lasing wavelength; α_2 represents the normalized losses; α_0 and α_s are parameters describing CNT saturable absorber; δ is the ellipticity of the pump wave, $\varepsilon=\tau_p/\tau_{Er}$ is the ratio of the the photon lifetime in the cavity τ_p to the lifetime of erbium ions at the first excited level τ_{Er}; $\chi_{p,s}=(\sigma_a^{(s,p)}+\sigma_e^{(s,p)})/\sigma_a^{(s,p)}$,($\sigma_a^{(s,p)}$ and $\sigma_e^{(s,p)}$ are absorption and emission cross-sections at the lasing (s) and pump (p) wavelengths); Δ is the detuning of the lasing wavelength with respect

to the maximum of the gain spectrum (normalized to the gain spectral width), β is the birefringence strength (2 $\beta=2\pi L_c/L_b$, L_b is the beat length and L_c is the cavity length), We use an approximation in Eqs. (5) that the dipole moments of the absorption and emission transitions for erbium-doped silica are located in the plane orthogonal to the direction of the light propagation. This approximation results in the angular distribution of the excited ions n(θ), which can be expanded into a Fourier series as follows [3]:

$$\boldsymbol{n(\theta)=\frac{n_0}{2}+\sum_{k=1}^{\infty} n_{1k}\cos(k\theta)+\sum_{k=1}^{\infty} n_{2k}\sin(k\theta)},$$

$$\boldsymbol{f_1=\left(\chi\frac{n_0}{2}-1\right)+\chi\frac{n_{12}}{2},\ f_2=\left(\chi\frac{n_0}{2}-1\right)-\chi\frac{n_{12}}{2},\ f_3=\chi\frac{n_{22}}{2}.} \quad (9)$$

To obtain results shown in Figs. 4, we used the following parameters: a), d), g) I_p =25, a=0.001 ; b), e), h) I_p =22, a=0.02; c), f), i) I_p =30, a=10. The other parameters: a)-i) $\beta_L=\beta_C=0,\ \alpha_1=5.38, \alpha_2=1, \alpha_s=10^{-3},\ \alpha_0=0.136, \delta=0.99$ (elliptically polarized pump SOP), Δ=0.13 $\varepsilon=10^{-4}$, χ_p=1, χ_s=2.3, Ω=0.005p, ϕ_0 =0, Ψ=π/2. To model the effect of the output POC transformation caused by the patchcord connect to the polarimeter, we use the following 3D rotation (around axes related to the Stokes parameters S_0, S_1, S_2, S_3) matrix [3]:

$$\begin{pmatrix}\tilde{S}_1\\ \tilde{S}_2\\ \tilde{S}_3\\ \tilde{S}_0\end{pmatrix}=\begin{bmatrix}a_{11} & a_{12} & a_{13} & 0\\ a_{21} & a_{22} & a_{23} & 0\\ a_{31} & a_{32} & a_{33} & 0\\ 0 & 0 & 0 & 1\end{bmatrix}\begin{pmatrix}S_1\\ S_2\\ S_3\\ S_0\end{pmatrix},$$

$$\boldsymbol{a_{11}=\cos(\psi)\cos(\gamma),\ a_{12}=\cos(\gamma)\sin(\alpha)\sin(\psi)-\cos(\alpha)\sin(\gamma),}$$
$$\boldsymbol{a_{13}=\cos(\alpha)\cos(\gamma)\sin(\psi)+\sin(\alpha)\sin(\gamma),}$$
$$\boldsymbol{a_{21}=\cos(\psi)\sin(\gamma),\ a_{22}=\cos(\alpha)\cos(\gamma)+\sin(\alpha)\sin(\psi)\sin(\gamma),}$$
$$\boldsymbol{a_{23}=-\cos(\gamma)\sin(\alpha)+\sin(\psi)\sin(\gamma), a_{31}=-\sin(\gamma),\ a_{32}=\cos(\psi)\sin(\alpha),}$$
$$\boldsymbol{a_{33}=\cos(\alpha)\cos(\psi).} \quad (10)$$

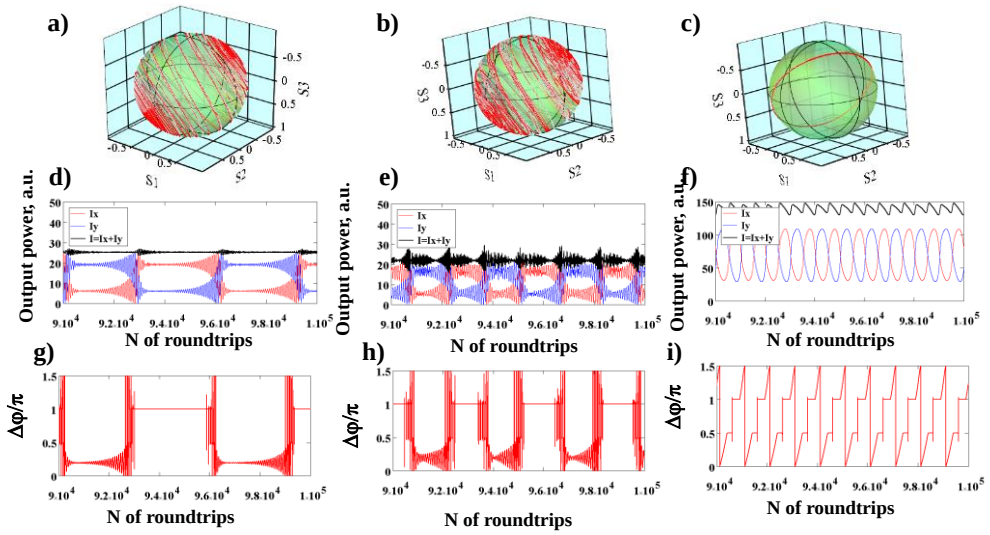

Fig. 4 Slow polarization dynamics of mode-locked fibre laser with the injected signal: a)- c) trajectories on the Poincaré sphere.); d) - f) The output power vs number of the round trips for two linearly cross-

polarized SOPs I_x (blue line) and I_y (red) and total power $I=I_x+I_y$ (black);); g-f) the phase difference (red) vs number of the round trips. Parameters: $\alpha = -\pi/4$, $\beta = \pi/4$, $\gamma = 2\pi/5$, (a-i); I_p =25 (a, d, g), I_p =22 (b, e, h); Ip=30 (c, f, i). The time span of 10^4 corresponds to 1 ms.

As follows from Fig. 4 (a-h), the injected signal with oscillating SOP modifies the spiral attractor and polarization dynamics of the polarization components x and y. The obtained theoretical results are quite close to the experimental data shown in [3]. With increasing the amplitude of the injected signal from a=0.02 to a=10, the polarization dynamics takes a completely different form, as shown in Fig. 4 (c, f, i). The spiral attractor is transformed to the circle (Fig. 4 c)), and x and y components' oscillations take the form of antiphase close to harmonic oscillations with the faster phase difference switching (Fig. 4 (f, i)). The dynamics is quite close to the experimental results shown in Ref. [3].

Conclusion

- Based on the experimental results and results of the theoretical modelling, we concluded that the analysis of HML based on the excitation of torsional-radial (TR_{2m}) acoustic mode provides just a qualitative approach to the linewidth suppression.
- Quantification of the linewidth suppression at the fundamental and 293.16 MHz, 464.17 MHz, 549.7 MHz harmonic frequencies demonstrated in the experiment [1] would require an improved jitter model that accounts for the state of polarization, dispersion, and contribution of phonons excited by this comb through the electrostriction effect.
- The results of modelling polarisation dynamics of NPR-based mode-locked fibre laser are close to the experimental data [2].
- The obtained results on controllable by the signal injection the sates of polarisation can be of interest for different application including data storage, spectroscopy, metrology and biomedical diagnostics (see Refs. In [3]). For example, the controllable number of pulses can advance the multi-pulse spectroscopy and distance ranging. Also, the controllable dynamic state of polarization enables the comb laser functionality to detect the object texture or biological tissue malformations based on detecting polarization signatures (see Refs. In [3]).

Next steps are following:

- ESR4 will support activity on using TR_{2m} acoustic mode-based HML for development of a high frequency dual -comb source.
- ESR4 continue activity on modelling polarisation dynamics of NPR-based mode-locked fibre laser.
- ESR4 will use Rsoft OPTSIM software and experimental data provided by ESR5 (D4.1) for development test of a new model of ellipsometric dual-comb laser source.

Publications

1. Sergeyev, S., Kolpakov, S. and Loika, Y., 2021. Vector harmonic mode-locking by acoustic resonance. Photonics Research, 9(8), pp.1432-1438. https://www.osapublishing.org/prj/fulltext.cfm?uri=prj-9-8-1432
2. Z. Huang, S. Sergeyev, Q. Huang, Z. Xing, Z. Yan, and Ch. Mou, Breathers driven by polarization instabilities, In CLEO: Applications and Technology (pp. JW3B-47). Optica Publishing. Group. https://publications.aston.ac.uk/id/eprint/43864/1/Huang_Sergeyev_et_al_Nonlinear_Polarization_Rotation_CLEO_2022_SES_v1.pdf

3. Sergeyev, S.V., Eliwa, M. and Kbashi, H., 2022. Polarization attractors driven by vector soliton rain. Optics Express, 30(20), pp.35663-35670. https://opg.optica.org/DirectPDFAccess/1AB4AB93-74A0-4EA1-B876C2B0FAFA056D_502636/oe-30-20-35663.pdf?da=1&id=502636&seq=0&mobile=no

This Project has received funding from the European Union's Horizon 2020 research and innovation programme under the Marie Sklodowska-Curie grant agreement No 861152